water

MDPI

Article

Laboratory Investigation on the Hydrodynamic Response of a Draft Varying Floating Breakwater (and Wave Energy Converter)

Sara Russo [1], Pasquale Contestabile [1,2], Diego Vicinanza [1,2,3,*] and Claudio Lugni [3]

[1] Department of Engineering, Università degli Studi della Campania "L. Vanvitelli", Via Roma, 29, 81031 Aversa, Italy; sara.russo@unicampania.it (S.R.); pasquale.contestabile@unicampania.it (P.C.)
[2] Inter-University National Consortium for Marine Sciences (CoNISMa), Piazzale Flaminio, 00144 Rome, Italy
[3] National Research Council of Italy, Institute of Marine Engineering, Via di Vallerano 139, 00128 Roma, Italy; claudio.lugni@cnr.it
* Correspondence: diego.vicinanza@unicampania.it

Abstract: The main purpose of this paper is the investigation of the feasibility of a novel hybrid module specifically designed for the Mediterranean Sea. This module is intended to work as an offshore floating breakwater in severe sea states, and alternatively as a wave energy converter in the more frequent mild sea states, depending on its level of submergence. An experimental campaign on a 1:10 module has been carried out in the wave tank of the University of Campania. The dynamic response of the device, as well as its hydraulic performances, was investigated under various wave conditions. The experimental results highlight the possibility of realizing and installing hybrid structures combining energy conversion and wave attenuation.

Keywords: hybrid floating breakwater-wave energy converter; laboratory experiments; multi-use device; transmission coefficient; offshore breakwater

Citation: Russo, S.; Contestabile, P.; Vicinanza, D.; Lugni, C. Laboratory Investigation on the Hydrodynamic Response of a Draft Varying Floating Breakwater (and Wave Energy Converter). *Water* **2024**, *16*, 445. https://doi.org/10.3390/w16030445

Academic Editor: Wencheng Guo

Received: 29 December 2023
Revised: 22 January 2024
Accepted: 25 January 2024
Published: 29 January 2024

1. Introduction

To unlock the promising blue energy market potential in the Mediterranean Sea and develop technologies that can be globally exported, it seems crucial to guarantee solutions effectively optimized for this closed basin. Among stand-alone systems or blue energy farms, a new solution is emerging to boost offshore energy harvesting in the Mediterranean area: the floating energy archipelago. It represents a multi-use energy hub for exploiting marine renewable energy with the possibility of combined and/or co-located solutions to reduce the variability of the power output, among other benefits [1].

The solution, proposed by the National Research Council of Italy, facilitates the implementation of various technologies for the generation of clean energy such as solar islands [2] and offshore wind farms [3]. The entirety of the produced energy can be stored and used to support the development of new productive activities, such as aquaculture, seawater desalination, and H_2 production. All these installations are spatially closed and protected by an array of floating breakwater modules. Implementing the twofold use of these modules, as an offshore breakwater and wave energy converter (WEC), is an interesting challenge. To achieve this, variable submergence (draft) is required. In more frequent mild sea states, the floating breakwater assumes the function of a wave energy converter, contributing to the energy production of the archipelago. In this configuration, the maximum energy is harvested when the floating module motions are in resonance with the waves (low draft). Otherwise, in extreme and severe sea states, it should strictly work as a passive breakwater, absorbing the incoming waves and protecting the devices installed in the archipelago. For the latter case, the module is filled with seawater to obtain a larger draft, increasing its stability.

Floating breakwaters (FBs) represent a category of maritime defenses usually known as "unconventional". Since 1811, when the first concept of a wooden floating breakwater was

proposed to protect Plymouth Sound [4], engineers and researchers have shown a growing interest in the topic due to the significant benefits obtainable through their use compared to their fixed, traditional counterparts [5]. Traditionally, they are classified depending on their shape: box type, pontoon type, frame type, mat type, tethered floating type, and horizontal-plate type [6]. Considering their wave attenuation mechanism, floating breakwaters are mainly represented by reflective and dissipative types [7]. Reflective breakwaters reflect the incoming wave and are often rigid structures that do not deform under the wave load. Dissipative breakwaters dissipate wave energy through turbulence, friction, and inelastic deformation. Thanks to their easy building process and durability, floating breakwaters have recently captured the attention of wave energy operators interested in developing and integrating their solutions over reliable and economic substructures, even in low-energy seas [8–10]. Currently, hybrid FBs are categorized based on the WEC-type system, as discussed in a recent review by Zhao et al., 2019 [11].

With the oscillating water column type WEC, a typical hollow-shaped structure is present. Examples of these devices can be found in [12–15], implementing one or more air chambers (each one equipped with an air turbine) to produce electricity. These studies demonstrated the possibility for these devices to function as WECs, but due to very low energetic performances, their main purpose remains coastal protection. In Michailides and Angelides, 2011 [16], a flexible floating breakwater consisting of several modules was proposed. The adjacent modules were connected by the power take-off (PTO hereinafter) system, which is driven by the relative motion of the modules.

With the "wave-activated bodies" or "oscillating bodies" type of WEC, some box-type breakwaters reached the stage of engineering application [17]. Pile-restrained floating breakwaters, modified with the insertion of a PTO system [18], have also been investigated. The performances of these devices were evaluated through linear potential flow theory by [19,20]. Another WEC-type coupled with pile-restrained breakwater is represented by the piezoelectric wave energy converter (PWEC), proposed in [21]. A hydro-elastic model has been developed to investigate the influence of width and submergence of the PWEC, showing that with increasing submergence, a shift towards large wave frequency occurs [22]. Their technological readiness level is lower, although the potential to be adapted for double use seems higher. However, long wave attenuation in operational conditions represents a crucial disadvantage.

A simple solution could arise by coupling WECs on the weather side of FBs [23–27]. In these cases, higher efficiency could be reached, and often arrays of WECs are used, making the modular WEC smaller in size compared to the breakwater behind it. Moreover, a significant increment in the efficiency of the WEC array can be observed due to the existence of the rear breakwater, reflecting the incoming waves, and amplifying the motion of the WECs [28]. It is noteworthy that, for specific frequencies, devices positioned on the weather side of a breakwater may experience zero energy efficiency due to Bragg resonance [29]: however, a proper triggering of the system can have a constructive effect [30,31].

The innovative hybrid FB-WEC analyzed in this paper has been proposed, simultaneously drawing inspiration from both Salter's duck [32] and traditional naval hull architecture [33,34]. The duck falls under a class of WECs known as terminators. A terminator is oriented perpendicularly to the direction of the wave. For the twofold function, a terminator is the best solution since it acts by destroying the waves it faces, leaving an almost calmer sea on the lee side. The updates proposed for the novel device act in accordance with the principles of versatility and cost-effectiveness.

In this paper, results derived from an experimental campaign on the hybrid device are analyzed on a 1:10 Froude-scaled module. The investigation mainly aimed at evaluating the dynamic behaviour of the device, the mooring loads, as well as its hydraulic performances in terms of wave transmission. The role of the draft parameter in determining the dual functioning is examined. In particular, in Section 2, the innovative device is accurately described, as well as the entire experimental setup. Section 3 reports the main results obtained and is followed by Section 4, where a discussion on the feasibility of the dual

function of the module is reported. Conclusions and future research lines on the module are described in Section 5.

2. Materials and Methods

In the first part of this section (Section 2.1), the concept, geometric properties, and inertial characteristics of the hybrid module are described. Following that, a brief overview of the physical model is provided in Section 2.2, outlining the properties and layout of the Floater and mooring. Subsequently, in Section 2.3, information about the facility, instruments, and the generation and acquisition system is presented. The final part, Section 2.4, offers a summary of the experimental test program.

2.1. Description of the Device

Transitioning from existing solutions that integrate a floating breakwater and a wave energy converter, we present an innovative hybrid system. The primary feature of the device is its adjustable submergence, enabling a dual function as both a passive breakwater and a wave energy harvester. Depending on sea-state conditions, the floater's draft is altered to modify overall stability.

In extreme and severe sea states, the device strictly functions as a passive breakwater, absorbing incoming waves and safeguarding the devices installed inside the archipelago. Conversely, in more frequent mild sea states, the floating breakwater acts as a wave energy converter (WEC), contributing to the energy production of the archipelago. In the latter case, maximum energy is harvested when the floating module moves in resonance with the waves. Water pumps inside the module facilitate displacement modification. In breakwater functionality, the module is almost fully submerged, ensuring (i) significant device stability and (ii) substantial reflection and dissipation of incoming waves. However, when the module operates as a WEC, a lower displacement is required, allowing for greater instability and device motion. Although the overtopping volume behind the structure may be higher when the device is almost fully submerged, this aspect does not significantly impact wave transmission, as the device is designed for offshore applications where there are no sensitive structures in close proximity to the breakwater.

The preliminary concept of the proposed floating breakwater-wave energy converter (FB-WEC) has been designed as a truncated lower cylinder, developing longitudinally and connected to an upper trapezoid. In WEC conditions, only the lower part of the module directly interacts with waves, and the choice of the cylinder is influenced by the expectation of achieving maximum motion exploitation. Experimental and numerical studies [35,36] comparing three different geometries demonstrated that the cylinder configuration exhibited large peak-to-peak roll amplitudes, associated with the smallest values of added mass moment of inertia [37]. In breakwater conditions, the enlargement of the body surface interacting with waves ensures greater stability. The reference system is centred on the keel line of the device, as illustrated in Figure 1, with the free surface tangent to the keel. When varying the draft, the free surface is envisioned as moving along the positive z-axis.

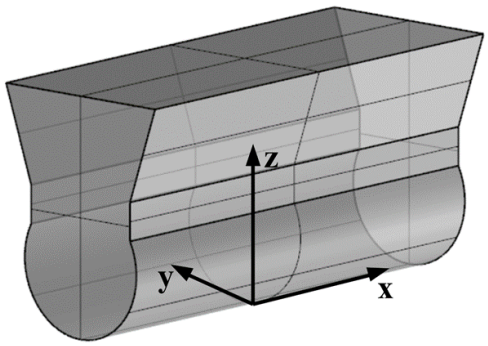

Figure 1. Coordinate system origin.

Different operational conditions were analyzed by considering four drafts, as shown in Figure 2. The device was gradually filled with water and consequently, its draft increased, aiming to provide rising stability.

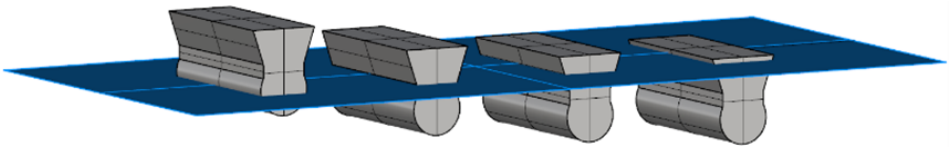

Figure 2. Sketch of the drafts. From left to right: 1.25 m, 2.5 m, 3.5 m, 4.75 m. The first two refer to a WEC functioning, while the third and fourth simulate a breakwater behaviour.

The most important stability parameter was the transverse metacentric height, denoted as GM_T, and defined as the distance between the vertical centre of gravity and the metacentre [38]. As shown in Figure 3, where the transversal section of a generic floater is represented, the metacentre is denoted asM_T. It is a fictitious point intersecting the vertical lines passing, respectively, from the centre of gravity, G, and the centre of buoyancy, B. For small heel angles, up to 10, the GM_T was assumed constant and followed Equation (1):

$$GM_T = KB + BM_T - KG \quad (1)$$

where BM_T is the distance from the metacentre to the centre of buoyancy B, also called metacentric radius; KB is the distance from the keel to the centre of buoyancy; and KG is the distance from the keel to the centre of gravity G. These parameters depended on the shape of the hull and the weight's amount and distribution. When varying the draft, D, they changed because the weight changed, and so did the submerged volume (hereinafter displacement ∇). Considering the double functioning of the device, the choice of the metacentric height fell into the values of 0.2 m for the WEC behaviour and 0.6 for protection purposes. Then, the centre of gravity was derived using Equation (1).

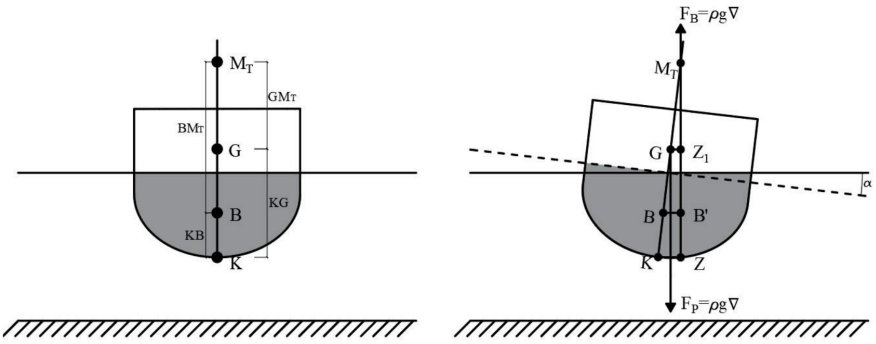

Figure 3. Parameters identification in zero condition and after heel angle.

In Table 1 the main parameters for each configuration are reported. It is worth noting that the four values of D were chosen as follows:

- D_1 = 1.25 m: in this case, the sea level reached half of the lower cylinder;
- D_2 = 2.50 m: referring to a condition in which the sea level embraced the whole cylinder;
- D_3 = 3.50 m: an intermediate condition, with the device submerged until the changing section;
- D_4 = 4.75 m: when the device was almost fully submerged.

These conditions suggest that the first two are associated with WEC behaviour, while the last two are indicative of breakwater performances.

In the full-scale scenario, the geometric characteristics of the device are detailed in Table 2. Here L represents the length in the x-direction, B is the overall beam, B_w is the waterline beam, R is the radius of the lower cylinder, H is the overall height and D is

the draft. Additionally, r_{xx}, r_{yy}, r_{zz} represent, respectively, the roll, pitch and yaw radius of gyration.

Table 1. Parametric properties for different operational conditions.

D [m]	GM_T [m]	KG [m]	∇ [m^3]
1.25	0.20	1.30	27.83
2.50	0.20	1.41	63.42
3.50	0.60	1.50	90.77
4.75	0.60	2.34	133.36

Table 2. Geometric parameters of different configurations.

Parameter	Unit
L [m]	10
R [m]	1.50
H [m]	5.00
B [m]	4.00
D_i [m]	1.25; 2.50; 3.50; 4.75
B_w [m]	2.96; 2.65; 2.99; 3.83
r_{xx}, r_{yy}, r_{zz} [m]	1.40; 2.50; 2.50

2.2. Experimental Setup

To accurately simulate the module's behaviour in mild and frequent sea states, a 1:10 scale model was constructed following Froude's law. The model (depicted in Figure 4a,b) was assembled using four shaped PVC sheets (density, $\rho = 1400$ kg/m^3): two for the side profiles, two for the trapezoidal forms and a cylindrical section with a 4 mm thickness. The sheets were secured by riveting slender steel profiles on the edges and siliconized for waterproofing. The upper part utilized the PVC sheet covering only one-third of the available surface for ease of manual ballasting/de-ballasting and to control inertia. Perforated bars on the side sheets served as connections for the anchoring system.

Dynamic testing was crucial to understand the effectiveness of the module, especially concerning resonance with waves, allowing for optimal energy harnessing. Attenuation performances were evaluated to determine effectiveness as a breakwater. Three draft values were explored: D_1 = 0.125 m, D_2 = 0.25 m, D_3 = 0.35 m.

(**a**) (**b**)

Figure 4. Lateral (**a**) and frontal (**b**) sections of the module in dry condition.

The main geometric and inertial characteristics of the floating platform are summarized in Table 3.

Four gravity anchors were used for the device, each connected to a mooring line, whose characteristics are reported in Table 4. The module was securely fastened with

four lines—two in the front and two behind the model. As depicted in Figure 5, each line comprised an inextensible rope of 1 m length, further connected to a system of four springs [39]. This arrangement was followed by a load cell, ultimately connected to the model through a 0.70 m long soft steel cable.

Table 3. Platform properties.

Parameter	Unit
R, Radius of the lower cylinder [m]	0.3
D_i, Draft [m]	0.125; 0.25; 0.35
CoG, Center of gravity below SWL [m]	0.01; −0.104; −0.17
m, Mass, including ballast [kg]	27.90; 63.40; 90.77
I_{44}, Roll Inertia [kg · m^2]	0.24; 0.54; 0.78
I_{55}, I_{66}, Pitch and Yaw Inertia [kg · m^2]	1.74; 3.96; 5.66

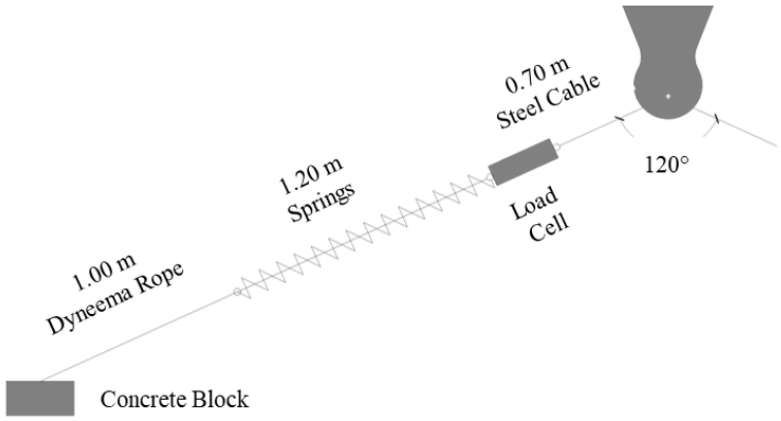

Figure 5. Sketch of the mooring system.

Table 4. Mooring lines properties

Parameter	Unit
Number of mooring lines	4
Horizontal Angle starboard-rear lines [°]	180
Vertical Angle floater- lines [°]	30
Vertical Angle starboard-rear lines [°]	120
Depth to anchors below SWL [m]	1.55
Depth to fairleads below SWL [m]	1.45; 1.38; 1.28
Radius to anchors from platform centreline [m]	3.25
Number of springs per line	4
Spring Pretension [kg]	0.7
Unstretched spring length [m]	1.16
Stretched spring length [m]	1.37
Equivalent springs extensional stiffness [N/mm]	0.033
Stretched mooring line length [m]	3.58; 3.53; 3.49

2.3. Test Facility and Instrumentation

The experimental campaign was conducted in a 3D tank measuring 16 m parallel to the wave paddle and 12 m in the other direction, with a depth range varying from 0.9 m to 0.43 m, resulting in a slope of 1:22. The tank was equipped with a dissipative beach in the final section, while a deeper area was constructed in the middle, measuring 5.50 m by 6.50 m parallel and orthogonal to the wavefront, with depths ranging from 1 m to 1.30 m. When the tank was filled with water, the pit had an average depth of 1.4–1.8 m.

The experimental campaign had two main objectives: evaluating the dynamics of the device and assessing its hydraulic performance in waves. The dynamics were examined

using an inertial measurement unit (IMU), capturing accelerations, angular velocities, and inclinations around the three axes [40]. Additionally, submersible in-line load cells were strategically placed on each mooring line to measure tension resulting from wave forces [41].

To record the wave profile, six resistive wave gauges were employed: three positioned in front of the model to measure reflection through the Mansard and Funke method [42], two behind the model for assessing transmission, and one outside the PIT to compare internal and external measurements. The arrangement of the probes and their coordinates with respect to the pit reference system is shown in (Figure 6) and detailed in Table 5.

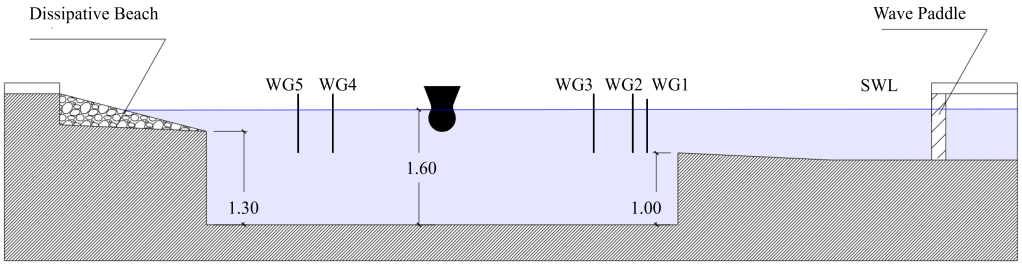

Figure 6. Section of the tank.

Table 5. Wave gauges coordinates, with respect to the pit.

WG	x_p [m]	y_p [m]
1	2.80	0.43
2	2.80	0.64
3	2.80	1.18
4	2.80	4.83
5	2.80	5.31
6	5.90	1.43

Regular and irregular waves were generated using the AwaSys 5 software [43], developed at the Hydraulics and Coastal Engineering Laboratory of the University of Aalborg (Denmark). For data acquisition, three different software programs were utilized: "WaveLab2" to record the elevation of the wave profile [44], the code provided with the IMU sensor to capture the movements of the device, and a LabVIEW (Laboratory Virtual Instrumentation Engineering Workbench, available at [45]) code to record the tension in the mooring anchors through the load cells. All acquired data, with a sampling frequency of 20 Hz, were synchronized, processed, and analyzed in MATLAB 2022b.

2.4. Experimental Test Program

The first part of the experimental test program was related to the calibration of the model. With the model properly identified, their behaviour under wave loads could be examined, in terms of dynamic by means of the response amplitude operators, in terms of loads on the mooring system, and in terms of attenuation performances through transmission coefficients.

2.4.1. Model Calibration

To achieve the desired properties of the model in terms of draft, KG, mass, and inertia, the model underwent several steps. Initially, it was weighed without ballast, and its centre of gravity and natural period in pitch and roll were determined (Figure 7a). Subsequently, preliminary tests were conducted in water to ascertain the model's properties, including static draft, trim, and heel. Inclining tests (Figure 7b) were performed for each draft value to establish the transverse metacentric height GM_T involving the measurement of the inclination angle recorded when moving a known mass m into different known positions Δy. The stability parameter was determined by solving Equation (2). Once the model

achieved the correct values of draft, trim, heel, and design weight, roll inertia was assessed by measuring the angular frequency in water using Equation (3).

$$m \cdot \Delta y = \rho \cdot \nabla \cdot GM_T \cdot sin(\alpha) \tag{2}$$

$$\omega_4 = \sqrt{\frac{\rho \cdot g \cdot \nabla \cdot GM_T}{I_{44} + A_{44}}} \tag{3}$$

(**a**) (**b**)

Figure 7. Measurements of properties in air (**a**) and in water (**b**).

To evaluate the restoring properties of the moored model, static tests were performed. Each mooring was pre-tensioned at 0.7 kg while the model was in the mean position. Subsequently, the model underwent a series of quasi-static displacements, evenly distributed along the positive and negative y-axis, and the corresponding mooring tensions were recorded.

2.4.2. Decay Test

Free oscillation tests were conducted on the moored model in the six degrees of freedom (surge, sway, heave, roll, pitch, yaw) to determine the natural periods and damping coefficients. The natural period T_N for each j-DoF was obtained by averaging the n-th cycles taken by the device to decay (Equation (4)). The damping coefficients a and b were found using the exponentially decaying sinusoidal equation (Equation (5)). Additionally, the damping ratio was determined using the logarithmic decrement method as a function of two response amplitudes x_i and x_{i+1}, according to Equations (6) and (7) [46]. In addition, the linear p_1 and quadratic p_2 damping coefficients were determined using a common method applied in the offshore industry [47], which involves linearly interpolating the left-hand side of Equation (8) over the coefficient multiplying p_2.

$$T_{N,j} = \sum_{i=1}^{n} T_i \tag{4}$$

$$x = a \cdot e^{-b \cdot t} \tag{5}$$

$$\zeta = \frac{\delta}{\sqrt{4 \cdot \pi^2 + \delta^2}} \tag{6}$$

$$\delta = \frac{1}{i} \ln \frac{x_i}{x_{i+1}} \tag{7}$$

$$\frac{2}{T_m} \cdot ln\frac{x_{i-1}}{x_{i+1}} = p_1 + p_2 \cdot \frac{16 \cdot x_i}{3 \cdot T_m} \tag{8}$$

2.4.3. Response under Wave Loads

Regular and irregular wave tests were conducted to assess the dynamic characteristics and attenuation performance of the device in all configurations. Specifically, the dynamic response was evaluated by defining the response amplitude operators (RAO) of the motions, as shown in Equation (9), where ξ_j represents the j-th DoF depending on the angular frequency ω , and a denotes the wave amplitude. The mooring response was assessed in terms of maximum and mean tensions T, along with their response amplitude operator, as described in Equation (10). On the other hand, the attenuation performances were appraised through the transmission coefficient K_T given in Equation (11), where, respectively, H_T and H_I represent the transmitted and incident wave heights. In the case of irregular waves, these wave heights are replaced by the corresponding spectral wave heights.

$$RAO_{\xi_j} = \frac{|\xi_j(\omega)|}{a} \tag{9}$$

$$RAO_{T_i} = \frac{|T(\omega)|}{a} \tag{10}$$

$$K_T = \frac{H_T}{H_I} \tag{11}$$

Table 6 provides an overview of the test matrix for the regular wave tests conducted on the model, involving three distinct wave steepness values denoted by ka. To further investigate the impact of draft variation on wave-module interaction, irregular wave tests were conducted. These irregular waves were generated using a JONSWAP spectrum [48] with a peak enhancement factor γ = 3.3 (Table 7).

Table 6. Regular wave tests.

T_p [s]	$ka = 0.075$	$ka = 0.15$	$ka = 0.2$
0.6	0.01	0.03	0.04
0.8	0.02	0.05	0.06
1.0	0.04	0.07	0.10
1.2	0.05	0.11	0.14
1.4	0.07	0.15	0.20
1.6	0.10	0.19	0.25
1.8	0.12	0.24	-

Table 7. Irregular wave tests.

T_p [s]	H_{m0} [m]
0.8	0.14
1.2	
1.6	
2.0	

3. Results

3.1. Model Calibration

The mass and inertia moments of the empty model were initially measured in air, with the mass equal to 11.72 kg. Subsequently, the floater was appropriately ballasted to achieve the desired centers of gravity, design drafts, trim, and heel (with the last two equal to zero). With the floater positioned in water, inclining tests were conducted to determine the transverse metacentric height of the device in different draft configurations, as explained in the previous section. Results are presented in Figure 8, where the slope

of the interpolant line for each draft represents the transverse metacentric height GM_T. The measured $GM_{T,M}$ values exhibit slight differences from the target values $GM_{T,T}$, as indicated in Table 8; however, these discrepancies are negligible.

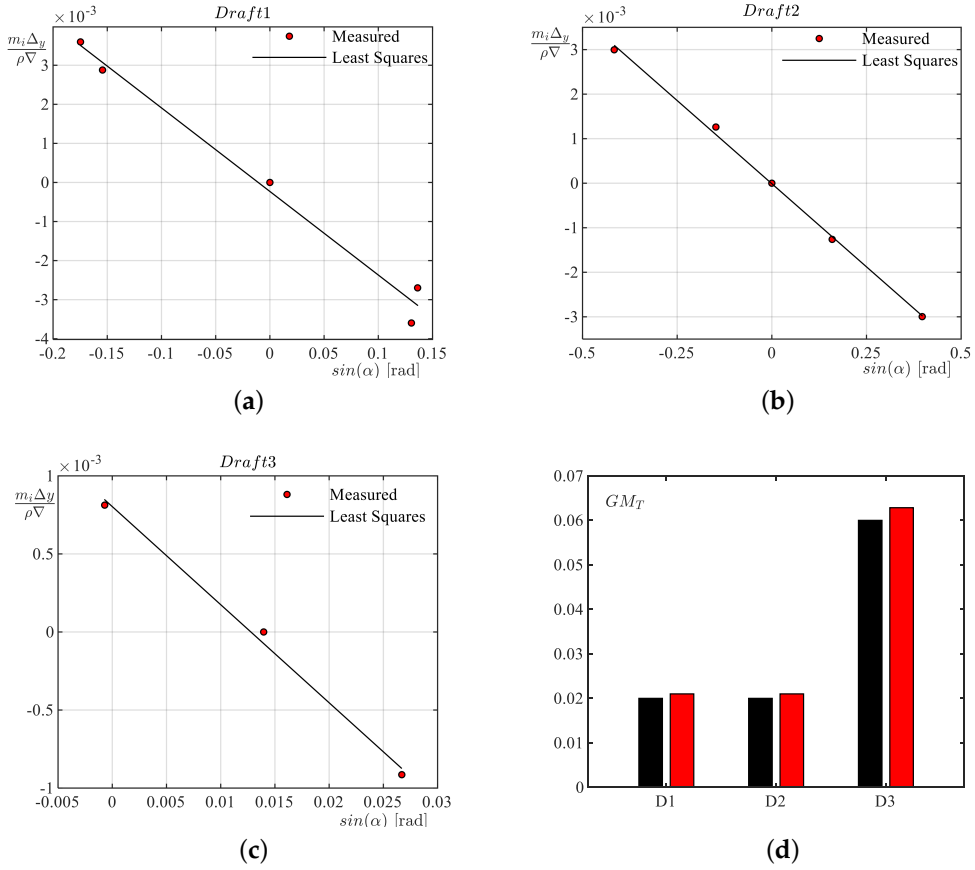

Figure 8. Results of the inclining tests: (**a**) in D_1, (**b**) in D_2, (**c**) in D_3, (**d**) differences between target (black bars) and measured values (red bars).

Table 8. Target and measured GM_T values.

Draft	$GM_{T,T}$	$GM_{T,M}$	$GM_{T,T}/GM_{T,M}$
D_1	0.02	0.021	1.05
D_2	0.02	0.021	1.05
D_3	0.06	0.063	1.05

3.2. Free Decay Tests

Free decay tests in calm water were conducted to assess the natural periods and damping coefficients. Initially, tests were performed without the mooring system, focusing on heave, roll, and pitch. Subsequently, the tests were repeated with the model anchored to examine any variations attributable to the mooring system. In this second condition, evaluations of surge, sway, and yaw DoFs were also possible. The results, including natural periods for both conditions, are presented in Table 9, along with an estimate of the percentage difference in measured natural periods, as expressed in Equation (12). As expected, the differences are nearly negligible.

$$\Delta T_N = \frac{T_N, unmoored - T_N, moored}{T_N, moored} \cdot 100 \quad (12)$$

Table 9. Natural periods in the six DoFs.

		Unmoored		Moored		ΔT_N
		T_N (s)	std (s)	T_N (s)	std (s)	(%)
D_1	Surge	-	-	11.28	1.28	-
	Sway	-	-	5.13	0.60	-
	Heave	0.79	0.03	0.74	0.00	−7.42
	Roll	2.26	0.34	2.19	0.40	−3.24
	Pitch	0.94	0.19	1.27	0.31	25.57
	Yaw	-	-	3.11	0.04	-
D_2	Surge	-	-	16.61	0.16	-
	Sway	-	-	8.61	0.16	-
	Heave	1.10	0.13	1.11	0.09	0.30
	Roll	1.48	0.07	1.54	0.03	4.15
	Pitch	1.30	0.05	1.27	0.03	−2.72
	Yaw	-	-	4.63	0.20	-
D_3	Surge	-	-	21.18	1.27	-
	Sway	-	-	10.55	0.31	-
	Heave	1.36	0.05	1.41	0.27	3.54
	Roll	1.18	0.03	1.16	0.05	−2.35
	Pitch	1.36	0.19	1.25	0.02	−8.25
	Yaw	-	-	5.28	0.39	-

A more detailed analysis was conducted for the roll rotation, a crucial motion for the dual functionality of the module. Figure 9 presents roll rotations, natural periods, and the definition of linear (p_1) and quadratic (p_2) damping coefficients for both unmoored and moored cases. The linear and quadratic damping coefficients, along with the a and b coefficients of the exponential decaying curve (Equation (5)) and the damping ratios (Equation (6)), are reported in Table 10. The latter confirms that the majority of the damping is linear, with p_1, for each draft, being at least 85 times higher than the quadratic p_2. The damping ratio of Equation (6) was evaluated as the mean value of the damping ratio observed for successive cycles. It was observed that for D_1 and D_3, its value remained almost constant with an increase in the cycles considered, around 4% in the first case and approximately 5.5% in the third. However, for the intermediate draft D_2, a decrease in the damping ratio was evident, starting from 4% in the first cycle and stabilizing around 2% after the 15th cycle.

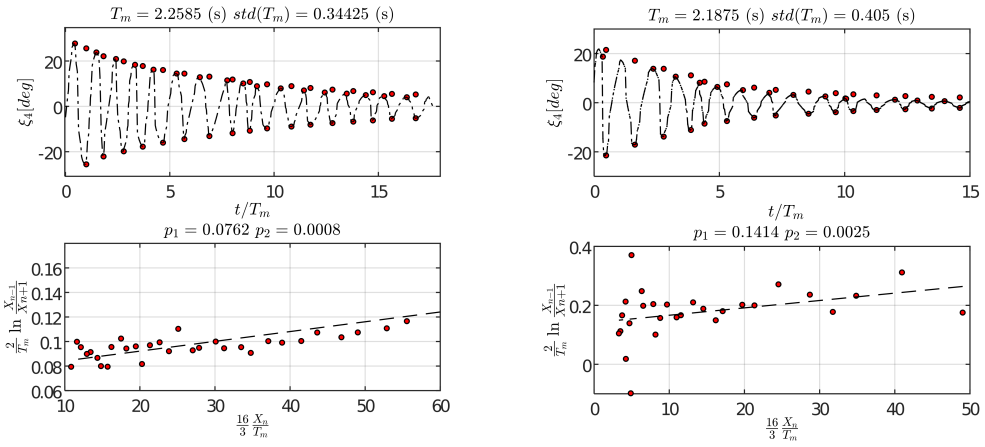

(**a**) (**b**)

Figure 9. *Cont.*

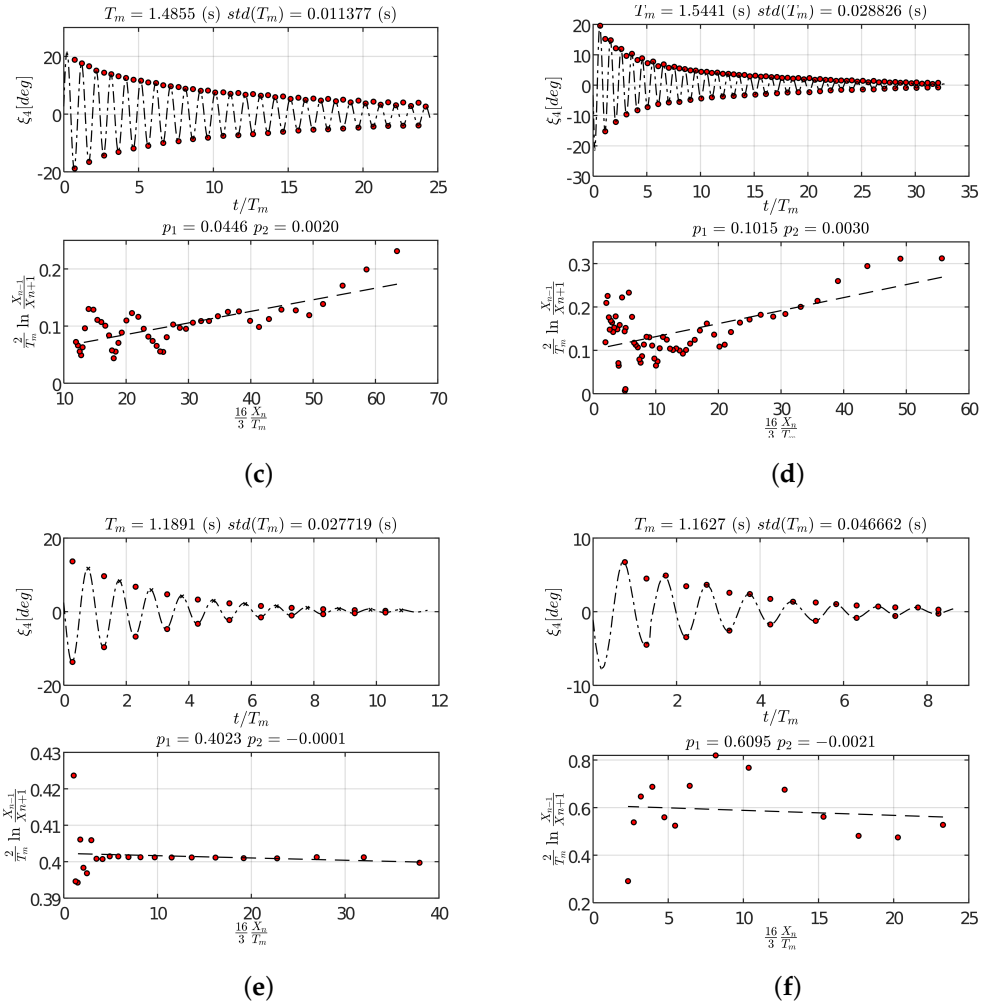

Figure 9. Measured decaying roll oscillation of the unmoored and moored structure (red circles), and corresponding damping coefficients p_1 and p_2 derived from the interpolation (dash black line) of Equation (8), respectively, for D_1 (**a**,**b**), D_2 (**c**,**d**) and D_3 (**e**,**f**).

Table 10. Roll damping coefficients and damping ratios.

	a	***b***	p_1	p_2	%
D_1	22.59	−0.09	0.14	0.0025	3.84
D_2	16.48	−0.08	0.10	0.0030	2.25
D_3	7.95	−0.29	0.61	−0.0021	5.59

3.2.1. Response under Wave Loads

To study the dynamic response of the model under regular waves, the response amplitude operators (*RAOs*) of the motions and the mooring line tensions were evaluated, while the transmission coefficient was used as an index for assessing the attenuation performances.

3.2.2. Dynamic Response

The heave and roll response amplitude operators of the floating device are plotted against λ/B_w (where λ is the wavelength) in Figure 10. They refer to regular waves with constant steepness (ka = 0.075), as indicated in Table 6. For both DoFs, it can be observed that the peak of the response occurs for wave periods close to the natural periods of the structure, marked with a red dashed line, respectively, for heave and roll, and for D_1 (a,b), D_2 (c,d), and D_3 (e,f).

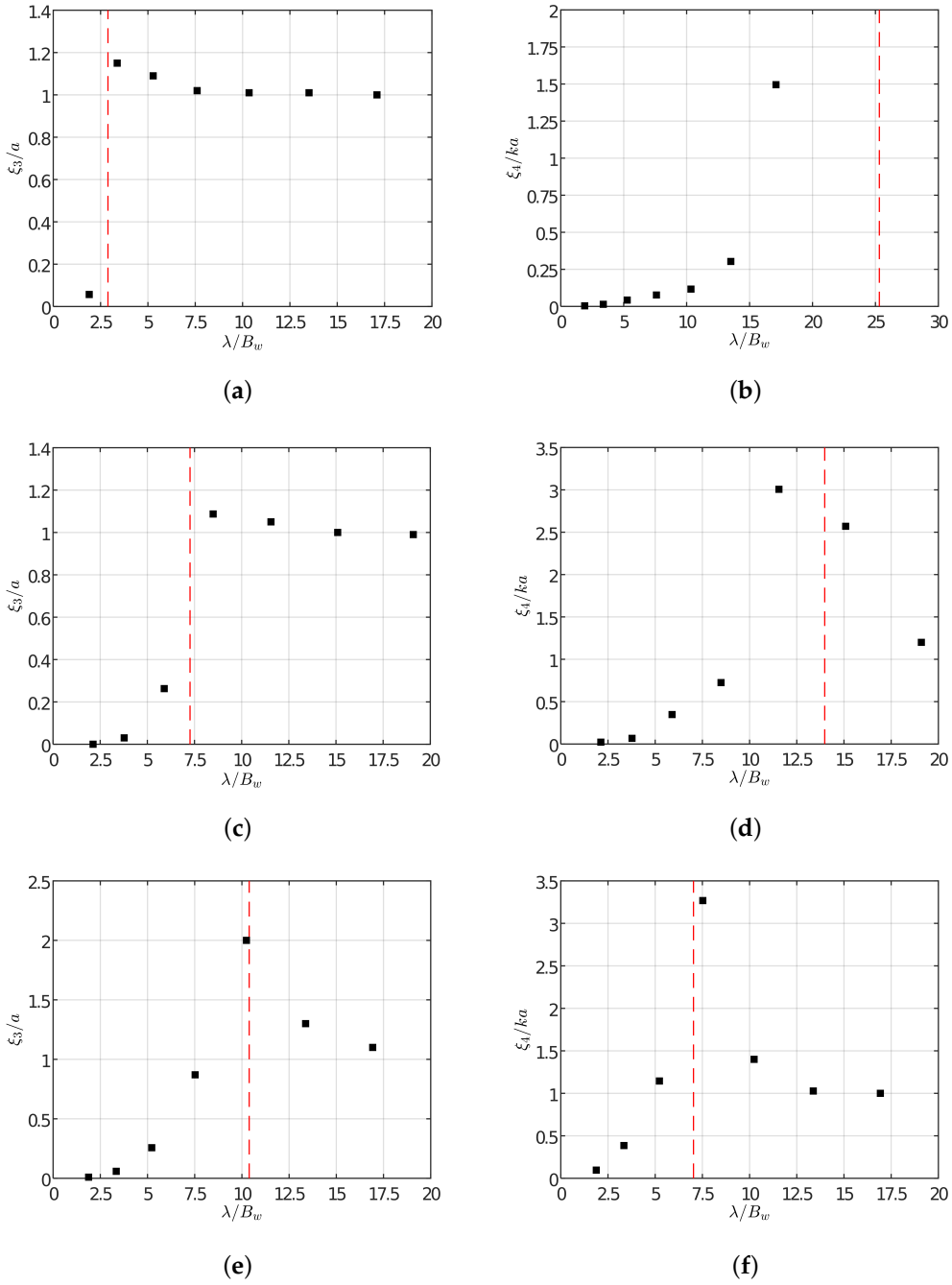

Figure 10. Heave and roll response amplitude operators (black squares) for D_1 (**a**,**b**), D_2 (**c**,**d**), and D_3 (**e**,**f**), in relation with the natural periods of the structure (red dashed lines).

3.2.3. Mooring Response

The maximum and mean tensions, along with the response amplitude operator obtained by dividing tension by wave amplitude, were utilized to assess the mooring response. The results are presented for one of the starboard lines and one of the rear lines in Figure 11, depicting maximum tensions in (a,b), mean tensions in (c,d), and the *RAOs* in (e,f) for the three draft configurations.

In general, it can be observed that maximum tension values, albeit slightly, increase with the wavelength in both the starboard and rear lines. Moreover, tensions assume very similar values for the cases of D_1 and D_2, while they markedly rise for D_3.

For the starboard line, the minimum mean tensions occur for the D_2 draft, becoming maximum in the rear line. This could be explained because of the minimum beam held by this draft configuration. The same behaviour, but with opposite results, is found for D_3, while for D_1 tensions stand in between for both lines.

Concerning the *RAOs*, for all the drafts and for both lines, values increase with the wavelength, being higher for D_1. However, their intensity is very low, as the mooring has been designed to respond in very long periods. If one considers the sway natural periods of Table 9 (hence λ/B_w), it can be seen that the smallest value occurs for D_1, followed by D_2 and D_3; this could explain the slope of the results.

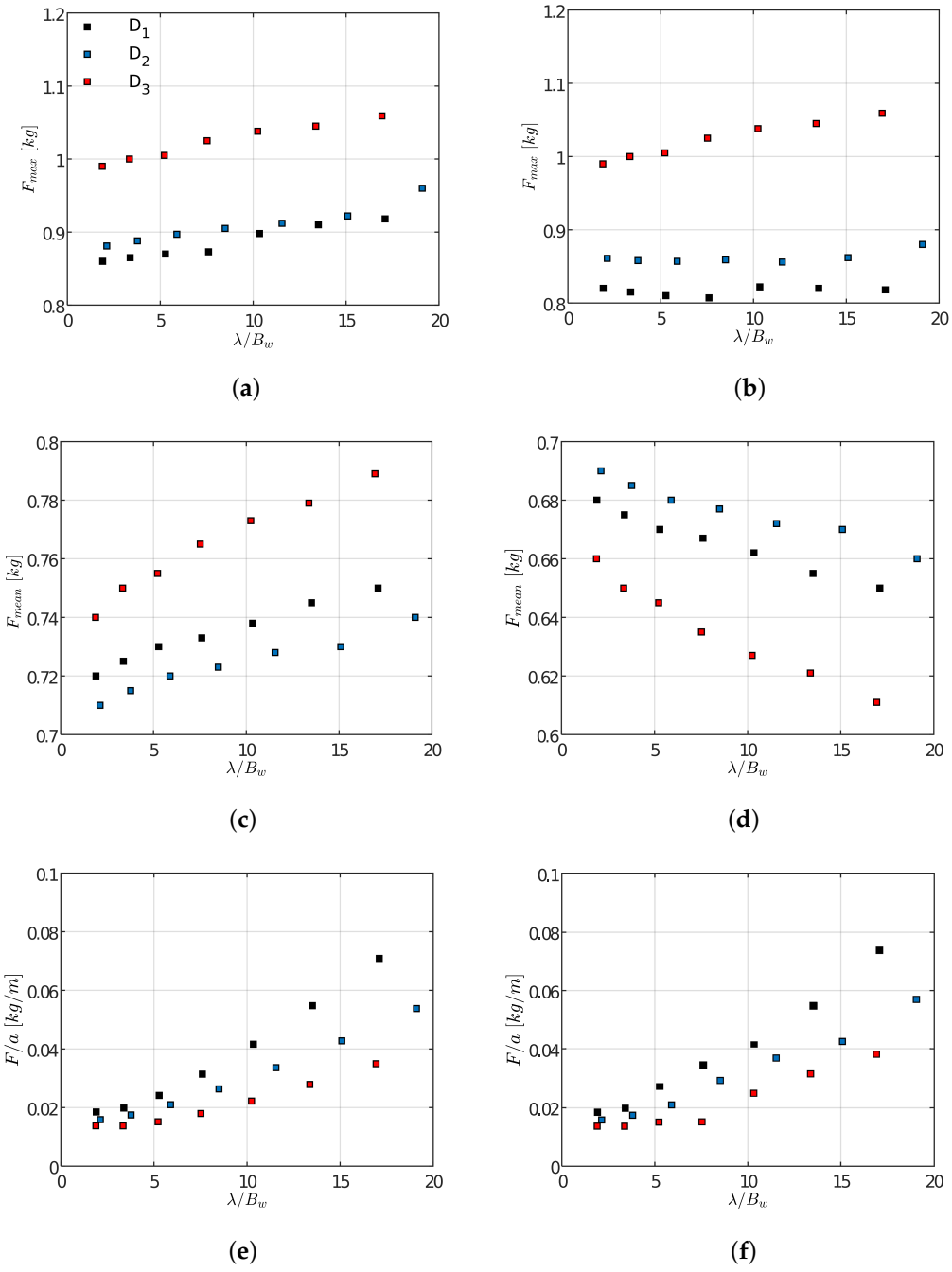

Figure 11. Mooring response for D_1, D_2, and D_3, respectively, for the starboard and the rear line: maximum tensions (**a**,**b**), mean tensions (**c**,**d**), and *RAOs* (**e**,**f**).

3.2.4. Transmission Coefficient

The transmission coefficient was computed for the three draft values and the three wave steepness values outlined in Table 6 (ka = 0.075; 0.15 and 0.20). As depicted in Figure 12, for the initial draft value, K_T achieved its maximum of 0.9 with the shortest wave, underscoring the efficacy of the module. With the increase in wave period (and height), the transmission coefficient exhibited a decline, reaching a minimum of 0.45 at T = 1.6 s. Furthermore, a marginal increase in K_T was observed with a rise in wave steepness. A disparate trend emerged for the second and third draft values, wherein the transmission coefficients, commencing from a minimum of 0.1 in the shortest waves, ascended until reaching peaks near the roll natural period of 1.6 s for D_2 and the heave natural period of 1.4 s for the third draft D_3. The sensitivity of the transmission coefficient to wave steepness was generally modest. However, for the D_2 case, the maximum values were attained at ka = 0.2, while for D_3, the same steepness resulted in the lowest K_T values, which were conversely maximal for ka = 0.15. In summary, the lowest K_T values transpired when the module assumed the third draft value, affirming its predisposition for employment in the floating breakwater function.

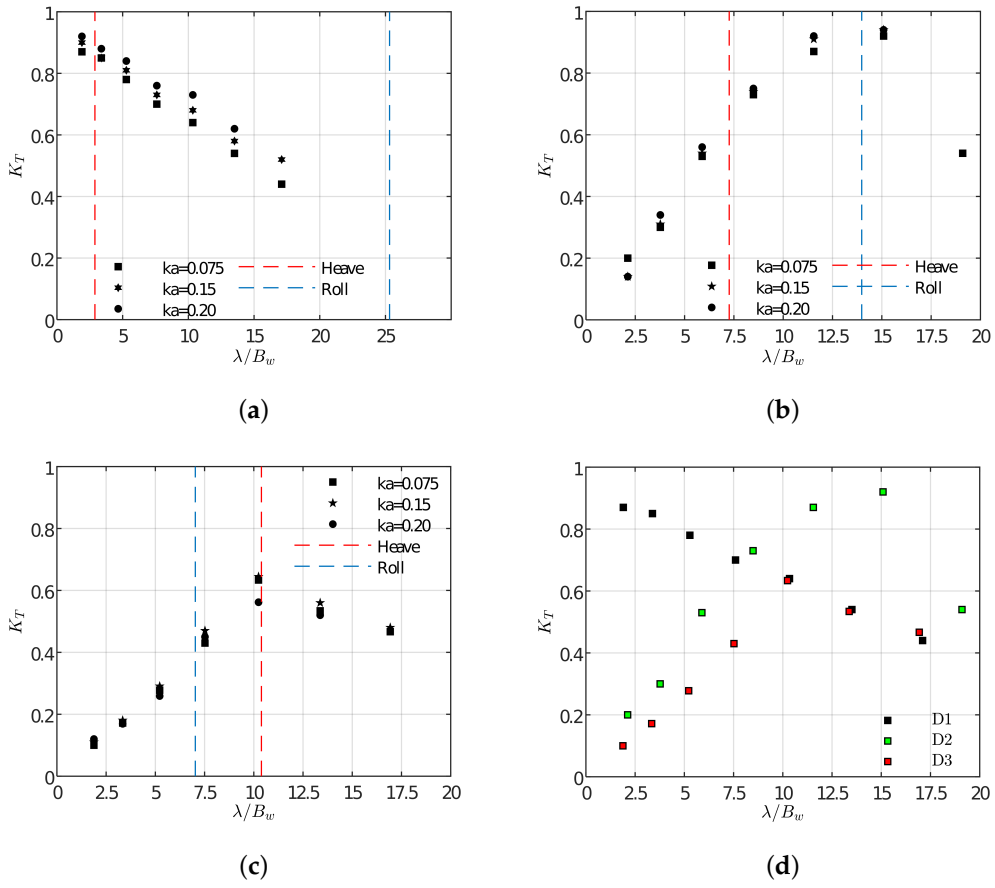

Figure 12. Transmission coefficient, for each draft varying steepness D_1 (**a**), D_2 (**b**), D_3 (**c**). In (**d**), transmission coefficients are reported for the three drafts with constant ka = 0.075.

4. Discussions

The experimental campaign aimed to investigate the influence of different draft configurations on the dynamic response and transmission coefficient of the floating module, that determine the operational range of functioning: wave energy converter and breakwater.

4.1. Dynamic

The effect of draft variations on the dynamic response of the device is analyzed through the examination of the response amplitude operator in roll, identified as the motion to be exploited to produce energy. The *RAOs* provide insights into the device's behaviour under regular wave conditions. Notably, the natural period of the system plays a crucial role in understanding the impact of draft changes on the dynamic response.

Regardless of the draft, a consistent response pattern is observed, reaching its maximum when the wave period is close to the natural period of the system (Figure 13). For the Mediterranean Sea conditions considered in this study, where typical wave periods range from 4–6 s for operational sea states and extend to 8–10 s for extreme conditions, the device exhibits optimal performances.

In particular, as reported in Table 11, the analysis reveals that draft D_2 experiences heightened response for operational sea states, making it more suitable for Wave Energy Conversion (WEC) purposes. On the other hand, draft D_3 operates away from resonance when functioning as a breakwater, indicating its effectiveness in protecting against extreme sea states.

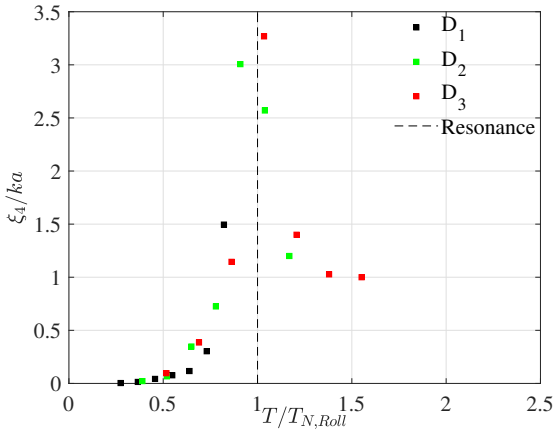

Figure 13. Roll *RAO* for the three Drafts.

Table 11. Typical periods for the Mediterranean Sea coupled with the motion of the structure.

$T_{p,FullScale}$ [s]	$T_{p,ModelScale}$ [s]	$T_p/T_{N,RollD_1}$	$T_p/\ T_{N,RollD_2}$	$T_p/T_{N,RollD_3}$
4	1.26	0.57	0.81	1.08
6	1.89	0.85	1.22	1.62
8	2.52	1.14	1.63	2.17
10	3.16	1.43	2.02	2.72

4.2. Attenuation

In general, an effective breakwater is capable of attenuating waves, exhibiting a low transmission coefficient (Equation (11)). To assess the module's efficacy in protecting the internal part of the archipelago depending on the draft D, the transmission coefficients obtained by analyzing regular and irregular waves from Tables 6 and 7 are compared. Specifically, in Figure 14, transmission coefficients for waves characterized by periods T = 0.8 s–1.2 s–1.6 s with varying wave heights (for regular waves), and with constant H_{m0} for irregular waves, are plotted against the parameter χ defined as:

$$\chi = \frac{T}{T_{N,heave}} \cdot \left(\frac{H-D}{H_{wave}}\right)^{0.25} \tag{13}$$

The parameter χ is dependent on the relative period between the waves and the heave natural period. In fact, as obtained in [49] for the π-type breakwater, the motion governing the transmission is also the heave for this module. Moreover, it is dependent

on the relative draft, also a crucial parameter in fixed structures [50]. A first observation relies on the distinction into two different zones, divided by the critical value of $\chi = 1.5$, strongly dependent on the heave natural period. Regular waves data follow two lines of opposite inclination with equations $K_T = 0.74 \cdot \chi - 0.34$ before the critical value and $K_T = -0.24 \cdot \chi + 1.26$ after this value, with R^2 being, respectively, 0.72 and 0.85.

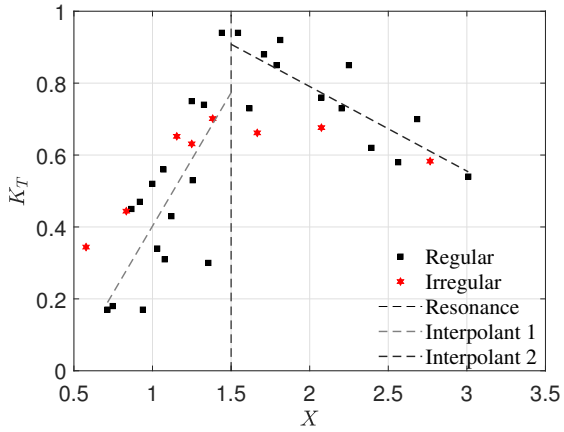

Figure 14. Transmission coefficient as a function of the parameter χ.

Moreover, differences between regular and irregular waves close to the critical value can be observed: irregular waves present lower values of transmission coefficients in that region, reasonably attributable to the distribution of the periods and wave heights characterizing an irregular wave.

5. Conclusions

This paper presents an innovative hybrid floating breakwater-wave energy converter, proposed and tested in the wave tank of the Department of Engineering of the University of Campania "Luigi Vanvitelli". The novelty of this hybrid device is the optimization of both functionalities, wave energy harvester and floating breakwater, by varying its draft. In fact, although it has been already demonstrated the possibility for hybrid floating breakwaters to convert some wave energy into electricity, their main purpose remains the protection against storm waves. On the other hand, there exist few WECs for which attenuation performances (mainly aimed at coastal protection) have been assessed. Even in this case, the breakwater functioning is an added feature. The performances of the proposed device have direct implications on the practical possibility of creating an offshore energy hub, as it should reduce the wave agitation under severe wave conditions. Otherwise, in more frequent mild sea states, the floating module should behave as WEC, contributing to the energy production of the archipelago.

The experimental campaign examined a 1:10 Froude-scaled model, exploring three draft values exposed to a series of regular and irregular waves. The primary objectives were to assess the dynamic response under wave action, focusing on motions and tensions in the mooring lines, and to evaluate the hydraulic performances in terms of transmission coefficient.

The initial findings concern the dynamic and attenuation performances. The assessment of heave and roll motion response amplitude operators reveals that, for both, the peak of the response occurs for wave periods close to the corresponding heave and roll natural periods of the structure. This suggests the potential exploitation of one or both of these DoFs to produce energy: however, the selection of a Power-Take-Off (PTO) system becomes crucial to determine the module's effectiveness. Analyzing the efficiency and operating mechanisms of various existing PTOs seems to incline the decision towards the use of a gyroscopic system [51] or an integrated sloshing/OWC system [52]. This choice is fundamental since, depending on the energy conversion mechanism, the dynamics of the device, as well as its energy efficiency, could vary significantly.

Continuing within the domain of response amplitude operators, those of the mooring tensions, calculated by dividing tension by wave amplitude, exhibit a subtle increase with wavelength for all drafts, both in the starboard and rear lines. The curves show a gradual rise due to the anticipated peak in mooring response in proximity to the sway natural period, which has been intentionally designed to be significantly higher than wave periods, escalating from D_1 to D_3. In terms of maximum tensions, mooring lines experience heightened strain with increasing wavelength, assuming very similar values for the case of D_1 and D_2, while markedly increasing for D_3. Conversely, mean tensions reach their peak for the D_2 case, attributed to the higher waterline beam.

The estimation of the transmission coefficient on the model revealed a substantial dependency on the natural period of the structure. The coefficient exhibited an increasing trend as it approached the roll and heave resonance periods, reaching peak values of 0.87 for D_1, 0.92 for D_2, and 0.63 for D_3, followed by a subsequent decrease to a consistent minimum of approximately 0.45. Notably, a distinct behaviour was observed for the first draft value, where the transmission coefficient was maximal for the lowest λ/B_w value and decreased with its increase. This behaviour was qualitatively explained by considering the wave generation capability of the floater. Specifically, for D_1 = 0.125 m, the module's limited ability to impede incoming waves passing underneath, attributed to its small draft, contributed to the observed maximum KT at $\lambda/B_w < 10$. Conversely, for D_2 and D_3 cases, the transmission coefficient aligned with the heave and roll damping evolution, indicating a significant contribution from waves generated by floater motions. Overall, the third draft exhibited the lowest values of KT highlighting its effectiveness as a breakwater.

Excluding values corresponding to the resonance periods, transmission coefficients are relatively low, even lower considering irregular waves. However, considering that the maximum relative wavelength λ/B_w is around 20 (i.e., $\lambda \approx 6$ m), this result is expected, as floating breakwaters are known to function optimally in short waves. For this reason, a smaller-scale module properly arranged in an optimal layout should be tested. In fact, while optimizing the spacing could result in a significant reduction in the wave energy entering the archipelago when the module works as a breakwater, on the other hand, considering the wave energy converter behaviour, choosing a particular value of the spacing could enhance the effectiveness of the first line in producing energy. The back line could function as a wave maker, as the reflected wave combines with the incident wave [53,54].

In general, this study on an innovative floating breakwater-WEC confirms its potential in protecting multi-use offshore platforms, reducing the wave loads on each component, and supplying electricity to the platform by converting wave energy.

Author Contributions: S.R. and C.L.—conceptualization, methodology. S.R. and P.C.—investigation S.R., P.C. and C.L.—writing—original draft preparation, review and editing. C.L. and D.V.—supervision, draft reviewing and editing. All authors have approved the final article. All authors have read and agreed to the published version of the manuscript.

Funding: The authors acknowledge the financial support from the "Ricerca di Sistema" project (RSE, 1.8 "Energia elettrica dal mare"), by Ministry of the Environment and Energy Safety (MASE), CUP B53C22008560001.C.L also acknowledges the financial support by: Project funded under the National Recovery and Resilience Plan (NRRP), Italy, Mission 4 Component 2 Investment 1.3—Call for tender No. 1561 of 11.10.2022 of Ministero dell' Università e della Ricerca (MUR); funded by the European Union—NextGenerationEU. Award Number: Project code PE0000021, Concession Decree No. 1561 of 11.10.2022 adopted by Ministero dell'Università e della Ricerca (MUR), Italy, CUP, Italy B53C22004060006, Project title "Network 4 Energy Sustainable Transition—NEST". MUR-FOE-STRIVE " STRIVE—La scienza per le transizioni industriali, verde, energetica" funded by Ministry of University and Research (CUP B53C22010110001).

Data Availability Statement: The experimental data used in this study are available from the corresponding author upon reasonable request.

Conflicts of Interest: The authors declare no conflicts of interest.

References

1. Azzellino, A.; Lanfredi, C.; Riefolo, L.; De Santis, V.; Contestabile, P.; Vicinanza, D. Combined Exploitation of Offshore Wind and Wave Energy in the Italian Seas: A Spatial Planning Approach. *Front. Energy Res.* **2019**, *7*, 42. [CrossRef]
2. Keiner, D.; Salcedo-Puerto, O.; Immonen, E.; van Sark, W.G.J.H.M.; Nizam, Y.; Shadiya, F.; Duval, J.; Delahaye, T.; Gulagi, A.; Breyer, C. Powering an island energy system by offshore floating technologies towards 100% renewables: A case for the Maldives. *Appl. Energy* **2022**, *308*, 118360. [CrossRef]
3. Russo, S.; Contestabile, P.; Bardazzi, A.; Leone, E.; Iglesias, G.; Tomasicchio, G.R.; Vicinanza, D. Dynamic loads and response of a spar buoy wind turbine with pitch-controlled rotating blades: An experimental study. *Energies* **2021**, *14*, 3598. [CrossRef]
4. Stuart, W. On the Plymouth breakwater. In *Report of the 11th Meeting of the British Association for the Advancement of Science*; John Murray: London, UK, 1842.
5. Permanent International Navigation Association and Maritime Navigation Commission. Working Group 28. In *Breakwaters with Vertical and Inclined Concrete Walls*; Pianc: Bruxelles, Belgium, 2003.
6. Dai, J.; Wang, C.M.; Utsunomiya, T.; Duan, W. Review of recent research and developments on floating breakwaters. *Ocean Eng.* **2018**, *158*, 132–151. [CrossRef]
7. Permanent International Association of Navigation Congresses (PIANC). Floating Breakwaters: A Practical Guide for Design and Construction. 1994. Available online: https://www.pianc.org/publication/floating-breakwaters-a-practical-guide-for-design-and-construction/ (accessed on 10 January 2021).
8. Majidi, A.; Bingölbali, B.; Akpınar, A.; Iglesias, G.; Jafali, H. Downscaling wave energy converters for optimum performance in low-energy seas. *Renew. Energy* **2021**, *168*, 705–722. [CrossRef]
9. Contestabile, P.; Russo, S.; Azzellino, A.; Cascetta, F.; Vicinanza, D. Combination of local sea winds/land breezes and nearshore wave energy resource: Case study at MaRELab (Naples, Italy). *Energy Convers. Manag.* **2022**, *257*, 115356. [CrossRef]
10. Contestabile, P.; Russo, S.; Azzellino, A.; Cascetta, F.; Vicinanza, D. Operating and Extreme weather conditions for testing Offshore Devices at Marine Renewable Energy Lab (MaRELab). In Proceedings of the European Wave and Tidal Energy Conference, Bilbao, Spain, 3–7 September 2023; Volume 15. [CrossRef]
11. Zhao, X.L.; Ning, D.Z.; Zou, Q.P.; Qiao, D.S.; Cai, S.Q. Hybrid floating breakwater-WEC system: A review. *Ocean Eng.* **2019**, *186*, 106126. [CrossRef]
12. Neelamani, S.; Natarajan, R.; Prasanna, D.L. Wave interaction with floating wave energy caisson breakwaters. *J. Coast. Res.* **2006**, *22*, 745–749.
13. Koo, W. Nonlinear time—Domain analysis of motion-restrained pneumatic floating breakwater. *Ocean Eng.* **2009**, *36*, 723–731. [CrossRef]
14. He, F.; Leng, J.; Zhao, X. An experimental investigation into the wave power extraction of a floating box-type breakwater with dual pneumatic chambers. *Appl. Ocean Res.* **2017**, *67*, 21–30. [CrossRef]
15. Sundar, V.; Moan, T.; Hals, J. Conceptual design of OWC wave energy converters combined with breakwater structures. *Int. Conf. Ocean Offshore Arct. Eng.* **2010**, *49118*, 479–489.
16. Michailides, C.; Angelides, D.C. Wave energy production by a flexible floating breakwater. In Proceedings of the 21th International Offshore and Polar Engineering, Maui, HI, USA, 19 June 2011.
17. Com, M. Breakwater Beats the Weather at Holy Loch. 2017. Available online: https://www.maritimejournal.com/breakwater-beats-the-weather-at-holy-loch/470075.article (accessed on 10 May 2021).
18. Ning, D.; Zhao, X.; Goteman, M.; Kang, H. Hydrodynamic performance of a pile-restrained WEC-type floating breakwater: An experimental study. *Renew. Energy* **2016**, *95*, 531–541. [CrossRef]
19. Zhao, X.; Ning, D.; Zhang, C.; Kang, H. Hydrodynamic investigation of an oscillating buoy wave energy converter integrated into a pile-restrained floating breakwater. *Energies* **2017**, *10*, 712. [CrossRef]
20. Zhao, X.; Ning, D.; Zhang, C.; Liu, Y.; Kang, H. Analytical study on an oscillating buoy wave energy converter integrated into a fixed box-type breakwater. *Math. Probl. Eng.* **2017**, *2017*, 3960401. [CrossRef]
21. Zheng, S.; Meylan, M.; Zhang, X.; Iglesias, G.; Greaves, D. Performance of a plate-wave energy converter integrated in a floating breakwater. *Iet Renew. Power Gener.* **2021**, *15*, 3206–3219. [CrossRef]
22. Zheng, S.; Meylan, M.H.; Zhang, X.; Iglesias, G.; Greaves, D. Wave power extraction from a piezoelectric wave energy converter integrated in a pile-supported breakwater. In Proceedings of the 14th European Wave and Tidal Energy Conference (EWTEC), Plymouth, UK, 9 September 2021; p. 2385.
23. Zingale, G. Modular Floating Breakwater for the Transformation of Wave Energy. U.S. Patent 6,443,653, 24 September 2002.
24. Martinelli, L.; Ruol, P.; Favaretto, C. Hybrid structure combining a wave energy converter and a floating breakwater. In Proceedings of the International Offshore and Polar Engineering Conference, Rhodes, Greece, 26 January 2016; pp. 622–628.
25. Favaretto, C.; Martinelli, L.; Ruol, P.; Cortellazzo, G. Investigation on possible layouts of a catamaran floating breakwater behind a wave energy converter. In Proceedings of the 27th International Offshore and Polar Engineering Conference, San Francisco, CA, USA, 25 June 2017.
26. Ning, D.; Zhao, X.; Zhao, M.; Kang, H. Experimental investigation on hydrodynamic performance of a dual pontoon—Power take-off type wave energy converter integrated with floating breakwaters. *Proc. Inst. Mech. Eng. Part J. Eng. Marit. Environ.* **2018**, *233*, 991–999. [CrossRef]

27. Ning, D.Z.; Zhao, X.L.; Chen, L.F.; Zhao, M. Hydrodynamic performance of an array of wave energy converters integrated with a pontoon-type breakwater. *Energies* **2018**, *11*, 685. [CrossRef]
28. Zhao, X.L.; Ning, D.Z.; Liang, D.F. Experimental investigation on hydrodynamic performance of a breakwater-integrated WEC system. *Ocean Eng.* **2019**, *171*, 25–32. [CrossRef]
29. Ouyang, H.T.; Chen, K.H.; Tsai, C.M. Investigation on Bragg reflection of surface water waves induced by a train of fixed floating pontoon breakwaters. *Int. J. Nav. Archit. Ocean Eng.* **2015**, *7*, 951–963. [CrossRef]
30. Gao, J.; Ma, X.; Dong, G.; Chen, H.; Liu, Q.; Zang, J. Investigation on the effects of Bragg reflection on harbor oscillations. *Coast. Eng.* **2021**, *170*, 103977. [CrossRef]
31. Gao, J.; Shi, H.; Zang, J.; Liu, Y. Mechanism analysis on the mitigation of harbor resonance by periodic undulating topography. *Ocean Eng.* **2023**, *281*, 114923. [CrossRef]
32. Salter, S.H. Wave power. *Nature* **1974**, *249*, 720–724. [CrossRef]
33. Russo, S.; Lugni, C.; Contestabile, P.; Vicinanza, D. A Preliminary Design for a novel concept of Floating breakwater (. . . and WEC). In Proceedings of the 14th European Wave and Tidal Energy Conference, Plymouth, UK, 5–9 September 2021; ISSN 2309-1983.
34. Russo, S.; Lugni, C.; Contestabile, P.; Vicinanza, D. A Novel Hybrid Floating Breakwater-Wave Energy Converter Device: Preliminary Experimental Investigations. In Proceedings of the European Wave and Tidal Energy Conference, Bilbao, Spain, 3–7 September 2023; Volume 15. [CrossRef]
35. Clemente, D.; Rosa-Santos, P.; Taveira-Pinto, F.; Martins, P. Experimental performance assessment of geometric hull designs for the E-Motions wave energy converter. *Ocean Eng.* **2022**, *260*, 111962. [CrossRef]
36. Clemente, D.; Rodrigues, C.; Esteves, R.; Correia, J.; Pereira, A.M.; Ventura, J.O.; Rosa-Santos, P.; Taveira-Pinto, F.; Martins, P. Experimental Performance Analysis of a Hybrid Wave Energy Harvesting System Combining E-Motions with Triboelectric Nanogenerators. *J. Mar. Sci. Eng.* **2022**, *10*, 1924. [CrossRef]
37. Clemente, D.; Rosa-Santos, P.; Taveira-Pinto, F.; Martins, P. Influence of platform design and power take-off characteristics on the performance of the E-Motions wave energy converter. *Energy Convers. Manag.* **2021**, *244*, 114481. [CrossRef]
38. Techet, A.H. *Hydrodynamics for Ocean Engineers*; MITPRESS: Cambridge, MA, USA, 2004.
39. Distribuzione Immediata Molle. Springs. Available online: https://dim.molle.com/dettagli.asp?id=533 (accessed on 12 December 2021).
40. WitMotion Shenzhen Co. Inertial Measurement Unit. Available online: https://www.wit-motion.com/proztsz/43.html (accessed on 26 November2021).
41. Applied Measurements.In-Line Submersible Load Cell. Available online: https://appmeas.co.uk/products/load-cells-force-sensors/in-line-submersible-load-cell-dden/ (accessed on 1 March 2022).
42. Mansard, E.P.; Funke, E.R. The measurement of incident and reflected spectra using a least squares method. *Coast. Eng. Proc.* **1980**, *1980*, 154–172.
43. Meinert, P.; Andersen, T.L.; Frigaard, P. *AwaSys 6 User Manual*; Department of Civil Engineering, Aalborg University: Copenhagen, Denmark, 2011.
44. Frigaard, P.; Andersen, T.L.*Analysis of Waves: Technical Documentation for Wavelab 3*; Department of Civil Engineering, Aalborg University: Copenhagen, Denmark, 2014.
45. National Instruments. (n.d.). About NI. Available online: https://www.ni.com/it-it/about-ni.html (accessed on 28 December 2021).
46. Karimirad, M. *Offshore Energy Structures: For Wind Power, Wave Energy and Hybrid Marine Platforms*; Springer: Berlin/Heidelberg, Germany, 2014.
47. Faltinsen, O. *Sea Loads on Ships and Offshore Structures*; Cambridge University Press: Cambridge, UK, 1990; Volume 1.
48. Hasselmann, K.; Barnett, T.P.; Bouws, E.; Carlson, H.; Carwright, D.E.; Enke, K.; Ewing, J.A.; Gienapp, H.; Hasselmann, D.E.; Kruseman, P.; et al. Measurements of wind-wave growth and swell decay during the Joint North Sea Wave Project (JONSWAP). *Dtsch. Hydrogr. Z.* **1973**, *8*, 1–95.
49. Ruol, P.; Martinelli, L.; Pezzutto, P. Formula to predict transmission for π-type floating breakwaters. *J. Waterw. Port Coast. Ocean Eng.* **2013**, *139*, 1–8. [CrossRef]
50. Contestabile, P.; Crispino, G.; Russo, S.; Gisonni, C.; Cascetta, F.; Vicinanza, D. Crown wall modifications as response to wave overtopping under a future sea level scenario: An experimental parametric study for an innovative composite seawall. *Appl. Sci.* **2020**, *10*, 2227. [CrossRef]
51. Mattiazzo, G. State of the art and perspectives of wave energy in the Mediterranean sea: Backstage of ISWEC. *Front. Energy Res.* **2019**, **7**, 114. [CrossRef]
52. Zhang, C.; Ding, Z.; Chen, L.; Ning, D. Sloshing dynamics of liquid tank with built-in buoys for wave energy harvesting. *J. Fluids Struct.* **2022**, *113*, 103662. [CrossRef]
53. Gao, J.; Lyu, J.; Wang, J.; Zhang, J.; Liu, Q.; Zang, J.; Zou, T. Study on transient gap resonance with consideration of the motion of floating body. *China Ocean Eng.* **2022**, *36*, 994–1006. [CrossRef]
54. Gong, S.; Gao, J.; Mao, H. Investigations on fluid resonance within a narrow gap formed by two fixed bodies with varying breadth ratios. *China Ocean Eng.* **2023**, *37*, 962–974.